Noname manuscript No.
(will be inserted by the editor)

Measuring the Masses of Supermassive Black Holes

Bradley M. Peterson

Received: date / Accepted: date

Abstract Supermassive black holes reside at the centers of most, if not all, massive galaxies: the difference between active and quiescent galaxies is due to differences in accretion rate relative to the Eddington rate and thus radiative efficiency. In this contribution, methods for measuring the masses of supermassive black holes are discussed, with emphasis on reverberation mapping which is most generally applicable to accreting supermassive black holes and, in particular, to distant quasars where time resolution can be used as a surrogate for angular resolution. Indirect methods based on scaling relationships from reverberation mapping studies are also discussed, along with their current limitations.

Keywords active galactic nuclei · black hole · reverberation mapping

1 Introduction

As recently as 20 years ago, whether or not active galactic nuclei (AGNs) were powered by accretion onto supermassive black holes was widely regarded as an open question. The theoretical arguments supporting gravitational accretion as the primary source of power in AGNs were in place within a few years of the discovery of quasars (Zel'dovich & Novikov 1964; Salpeter 1964; Lynden-Bell 1969) and some two decades later Rees (1984) convincingly argued that supermassive black holes were the inevitable endpoint of *any* of the scenarios proposed to account for activity in galactic nuclei. But definitive observational proof remained illusive.

Now, however, it is now generally accepted that black holes reside at the center of most, if not all, massive galaxies, both quiescent and active. And, perhaps ironically, the first convincing proof of the existence of supermassive black holes was not in AGNs, but in quiescent galaxies. It was primarily the high angular resolution afforded by *Hubble*

B.M. Peterson
Department of Astronomy, The Ohio State University
Columbus, OH 43210 USA
Tel.: +1-614-292-2022
Fax: +1-614-292-2928
E-mail: peterson.12@osu.edu

Space Telescope that enabled determination of the masses of nuclear black holes; for the first time, the dynamics of stars and gas in the nuclei of nearby galaxies could be studied on scales smaller than the black hole radius of influence, $R_{\rm BH} = GM_{\rm BH}/\sigma_*^2$, where $M_{\rm BH}$ is the black hole mass, σ_* is the velocity disperion of the stars in the host-galaxy bulge, and G is the gravitational constant. Detection of supermassive black holes in quiescent galaxies showed that AGNs are different from other galaxies not because they harbor supermassive black holes in their nuclei, but because their supermassive black holes are actively accreting mass at fairly high rates, typically more than $\sim 0.1\%$ of the Eddington rate.

The realization that supermassive black holes are ubiquitous led to improved understanding of quasar evolution. The AGN population at the present epoch is a small fraction of what it was at its peak at $2 < z < 3$ or so. The quiescent supermassive black holes in most galaxies are clearly the remnants of the quasars of the distant past. The demographics of black holes (e.g., Shankar 2009; Vestergaard & Osmer 2009; Shen & Kelly 2012, and references therein) are thus of keen interest for understanding the accretion history of the universe.

2 Measuring the Masses of Supermassive Black Holes

2.1 Direct versus Indirect Methods

A distinction must first be drawn between *direct* and *indirect* methods of measuring black hole masses.

- Direct measurements are those where the mass is derived from the dynamics of stars or gas accelerated by the black hole itself. Direct methods include stellar and gas dynamical modeling and reverberation mapping.
- Indirect methods are those where the black hole mass is inferred from observables that are correlated with the black hole mass. This includes masses based on correlations between black hole masses and host-galaxy properties, such as the velocity dispersion of bulge stars, i.e., the $M_{\rm BH}$–σ_* relationship (Ferrarese & Merritt 2000; Gebhardt et al. 2000a; Tremaine et al. 2002), or the bulge luminosity, i.e., the $M_{\rm BH}$–$L_{\rm bulge}$ relationship (Kormendy & Richstone 1995; Magorrian et al. 1998), and masses based on AGN scaling relationships, such as the R–L relationship discussed in §5.1.

It is also common to distinguish among "primary," "secondary," and even "tertiary" methods, based on the number of assumptions and model dependence. Reverberation mapping (§3) is an interesting example: it is a *direct* method as it is based on observations of gas that is accelerated by the gravitational potential of the central black hole, but, as generally practiced, it is also a *secondary* method because absolute calibration of the mass scale depends on reference to another method. (see §4.1).

2.2 A Brief Summary of Primary Methods

2.2.1 Dynamics of Individual Sources

The most accurate and reliable mass measurements are based on studying the motions of individual sources that are accelerated by the gravity of the black hole. The most

well-determined mass, not surprisingly, is that of Sgr A* at the Galactic Center[1]. Two decades of observations of the proper motions and radial velocities of individual stars (e.g., Genzel, Eisenhauer, & Gillessen 2010; Meyer et al. 2012) enabled by the combination of advanced infrared detectors and adaptive optics on large telescopes, has led to a measurement of a black hole mass of $4.1(\pm 0.4) \times 10^6\, M_\odot$.

A second measurement of similar quality is that of the mass of the black hole in the galaxy NGC 4258 (a.k.a., M 106), which is a Type 2 AGN. In AGN unified models, Type 2 AGNs are those which are viewed at high inclination and are heavily obscured by the dusty molecular "torus" in the AGN midplane. In Type 2 sources, the broad lines and continuum that characterize the spectra of Type 1 AGNs are thus not directly observed. A consequence of observing the nucleus through a large column molecular gas is that under the right circumstances masers are formed, so bright that in this case they are called "megamasers." The proper motions and radial velocities of the individual megamaser sources in NGC 4258 show that they arise in a warped rotating disk around a black hole of mass $M_{\rm BH} = 3.78 \times 10^7\, M_\odot$ (Miyoshi et al. 1995).

Both of these cases are special in that they are, relatively speaking, very close, $\sim 8\,$kpc for the Galactic Center and $\sim 7.2\,$Mpc for NGC 4258. The black hole radius of influence is better resolved in these two galaxies than in any other (see Gültekin et al. 2009), in the former case simply because of its proximity and in the latter case also because the observations are made at $\sim 20\,$MHz, where it is possible to attain very high angular resolution with VLBI techniques.

2.2.2 Collective Motions

Black hole masses can also be determined by their gravitational effects on systems of stars or gas. The collective dynamics of stars or gas on scales of $R_{\rm BH}$ can be modeled, with the central $M_{\rm BH}$ a free parameter. An excellent review of these methods is provided by Ferrarese & Ford (2005).

Using stellar dynamics to determine black hole mases has the advantage that stars, unlike gas, respond to gravitational forces only. On the other hand, high angular resolution is required to resolve, or at least nearly resolve, $R_{\rm BH}$. Using gas dynamics has the advantage of being somewhat simpler, fundamentally because gas is viscous and settles into a rotating disk-like structure fairly quickly compared to the relaxation time for stars in a galactic nucleus. Also, at least in the case of reverberation mapping (§3), high angular resolution is not required.

Stellar dynamical modeling is based on the superpositioning of individual stellar orbits from a large orbit library to obtain a best fit to the observables, mainly the surface brightness profiles and line-of-sight velocity distributions. Several sophisticated computer codes for this have been developed (e.g., Gebhardt et al. 2003; van der Marel et al. 1998; Creeton et al. 1999; Thomas et al. 2004; Valluri, Merritt, & Emsellem 2004).

A small, but non-negligible, fraction ($< 20\,\%$; Tran et al. 2001) of early-type galaxies have small nuclear dusty disks. These are often found to be emission-line sources, so their Doppler motions can be detected. Their dynamics can be modeled with the

[1] The phrase "not surprisingly" in this context is used because Sgr A* is 100 times closer than any other supermassive black hole so it is possible to observe the motions of individual stars around the black hole in its vicinity. But the very fact that individual stars at the Galactic Center can be observed, despite 30 mag of visual extinction, was one of the things the author least expected to see in his own scientific lifetime.

central mass as a free parameter. This has enabled measurement of some of the largest known supermassive black holes (Macchetto et al. 1997; Bower et al. 1998; de Francisco, Capetti, & Marconi 2008; Dalla Bontà et al. 2009).

All together, the number of supermassive black holes whose masses have been determined by modeling stellar or gas dynamics numbers over 70 (McConnell & Ma 2013). This number is not likely to increase dramatically in the near term on account of the difficulty in resolving $R_{\rm BH}$ beyond the Virgo Cluster. However, reverberation mapping presents a viable alternative for measuring black hole masses at large cosmological distances via gas dynamics by substituting time resolution for angular resolution. The major limitation is that it is only applicable to Type 1 (broad emission-line) AGNs, a trace population, but one that was more predominant at higher redshift. Since the focus of this discussion is on accreting black holes, emphasis on reverberation mapping of AGNs does not seem misplaced.

3 Reverbation Mapping of AGNs

3.1 Beginnings

That the continuum emission from AGNs varies on quite short time scale has been known since nearly the time of the discovery of quasars. Indeed, within a few years of their discovery optical variability was regarded as a defining characteristic of quasi-stellar objects (Burbidge 1967). There were also some early scattered reports of *emission-line* variability (e.g., Andrillat & Souffrin 1968; Pastoriza & Gerola 1970; Collin-Souffrin, Alloin, & Andrillat 1973; Tohline & Osterbrock. 1976), which were in each case quite extreme changes; this is not surprising, given that only dramatic changes (e.g., apparent change from Type 1 to Type 2) could be detected with the technology of the times. With the proliferation of sensitive electronic detectors in 1980s, a strong connection between continuum and emission-line variability was established (Antonucci & Cohen 1983; Peterson et al. 1983; Ulrich et al. 1991, and references therein), though the initial results met with skepticism as the BLR appeared to be an order of magnitude smaller than predicted by photoionization theory (Peterson et al. 1985).[2] Nevertheless, an older idea (Bahcall, Kozlovsky, & Salpeter 1972) about how emission-line region structure could be probed by variability was cast into a mathematical formalism by Blandford & McKee (1982) and given the name "reverberation mapping."

[2] The discrepancy between theory and observation was due to an oversimplified theory; it was implicitly assumed in photoionization equlibrium modeling that all BLR "clouds" are intrinsically identical. A successful photoionization model was one that correctly predicted the emission-line intensity ratios in the emitted spectrum of some "standard" cloud. A key intensity ratio is C IV λ1549/C III] λ1909. Moreover, the very presence of C III] λ1909 set an upper limit to the density as this line is collisionally suppressed above $10^{9.5}\,{\rm cm}^{-3}$. The first high-sampling rate reverberation program (Clavel et al. 1991) showed that C IV λ1549 and C III] λ1909 arise at different distances from the central source, thus obviating the earlier arguments.

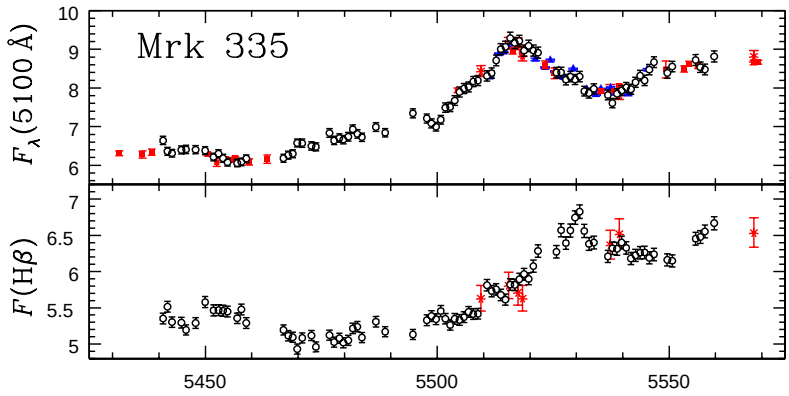

Fig. 1 Optical continuum (top) and broad Hβ emission-line (bottom) light curves for Mrk 335. The variations in Hβ follow those in the continuum by 13.9 ± 0.9 days. Grier et al. (2012a,2012b).

3.2 Theory of Reverberation Mapping

3.2.1 Assumptions

In this section, the basic theory of reverberation mapping is briefly outlined. More thorough discussions are available elsewhere (e.g., Peterson 1993, 2001).

Some very basic observations allow us to make several simplifying assumptions:

1. The emission lines respond rapidly to continuum changes (Figure 1), showing that the BLR is small (because the light-travel time is short) and the gas density in the BLR is high (so the recombination time is much shorter than the light-travel time). It is also noted that the dynamical timescale (of order $R_{\rm BLR}/\Delta V$) of the BLR is much longer than the reverberation timescale (of order $R_{\rm BLR}/c$), so the BLR is essentially stationary over a reverberation monitoring program.
2. The continuum-emitting region is so small compared to the BLR it can be considered to be a point source. It does *not* have to be assumed that the continuum emits isotropically, though that is often a useful starting point.
3. There is a simple, though not necessarily linear or instantaneous, relationship between variations of the ionizing continuum (at $\lambda < 912\,$Å) and the observed continuum (typically at $\lambda \sim 5100\,$Å). The fact the reverberation works at all justifies this at some level of confidence.

3.2.2 The Transfer Equation

Over the duration of a reverberation monitoring program, the continuum behavior over time can be written as $C(t) = \langle C \rangle + \Delta C(t)$ and the emission-line response as a function of line-of-sight velocity $V_{\rm LOS}$ is $L(V_{\rm LOS}, t) = \langle L(V_{\rm LOS}) \rangle + \Delta L(V_{\rm LOS}, t)$ where $\langle C \rangle$ and $\langle L(V_{\rm LOS}) \rangle$ represent mean values. On a reverberation timescale, both continuum and emission-line variations are usually rather small (typically $\sim$ 10–20%) so even if their relationship is non-linear, it can be modeled as linear on short timescales. In this case,

the relationship between the continuum and emission-line variations can be written as

$$\Delta L(V_{\rm LOS}, t) = \int \Psi(V_{\rm LOS}, \tau) \Delta C(t - \tau)\, d\tau, \tag{1}$$

which is usually known as the "transfer equation" and $\Psi(V_{\rm LOS}, \tau)$ is the "transfer function." Inspection of eq. (1) shows that $\Psi(V_{\rm LOS}, \tau)$ is the observed response to a δ-function continuum outburst.

3.2.3 Construction of a Velocity–Delay Map

The transfer function can be constructed geometrically as it is simply the six-dimensional phase space of the BLR projected into the observable coordinates, line-of-sight velocity (i.e., Doppler shift) and time delay relative to the continuum variations. It is therefore common to refer to the transfer function $\Psi(V_{\rm LOS}, \tau)$ as a "velocity–delay map." It should be clear that each emission line has a different velocity–delay map because the combination of emissivity and responsivity is optimized at different locations of the BLR for different lines. To map out *all* of the BLR gas would require velocity–delay maps for multiple emission lines with different response timescales.

Consider for illustrative purposes a very simple BLR model, a circular ring of gas orbiting counterclockwise at speed $v_{\rm orb}$ around the central source at a distance R. Suppose that a distant observer sees this system edge-on, as shown in the upper part of Figure 2, and define a polar coordinate system centered on the continuum source with the angle θ measured from the observer's line of sight. Two clouds are shown at positions $(R, \pm\theta)$. Photons from a δ-function continuum outburst travel toward the observer along the $-x$ axis. The dotted line shows the path taken by an ionizing photon from the same outburst will reach the BLR cloud pictured in the lower half of the figure after travel time R/c; an emission-line photon produced in response by the cloud and, by chance, directed toward the distant observer travels an additional distance $R\cos\theta/c$, where it is now the same distance from the observer as the continuum source. So relative to the ionizing photons headed directly toward the observer from the continuum source, the emission-line photons are delayed by the sum of these two dotted segments, i.e., by

$$\tau = (1 + \cos\theta)\, R/c. \tag{2}$$

The locus of points that all have the same time delay to the observer is labeled as an "isodelay surface" in the top part of the figure; a moment's reflection will convince the reader that the isodelay surface is a paraboloid. The corresponding Doppler shifts of the clouds at coordinate $(R, \pm\theta)$ are $\mp v_{\rm orb} \sin\theta$. These transformations are general, and a ring of radius R and orbital speed $v_{\rm orb}$ projects in velocity–delay space to an ellipse with axes $2v_{\rm orb}$ centered on $V_{\rm LOS} = 0$ and $2R/c$ centered on R/c. Here the ring is pictured edge-on, at inclination $90^{\rm o}$; at any other inclination i, the projected axes of the ellipse in velocity–delay space are correspondingly reduced to $2v_{\rm orb}\sin i$ and $2R\sin i/c$. Thus, a face-on ($i = 0^{\rm o}$) disk projects in velocity–delay space to a single point at $(0, R/c)$; all of the ring responds simultaneously and no Doppler shift is detected.

Generalization of this structure to a Keplerian disk is straightforward by simply adding more rings such that $v_{\rm orb} \propto R^{-1/2}$. This is illustrated for a system of several rings in Figure 3.

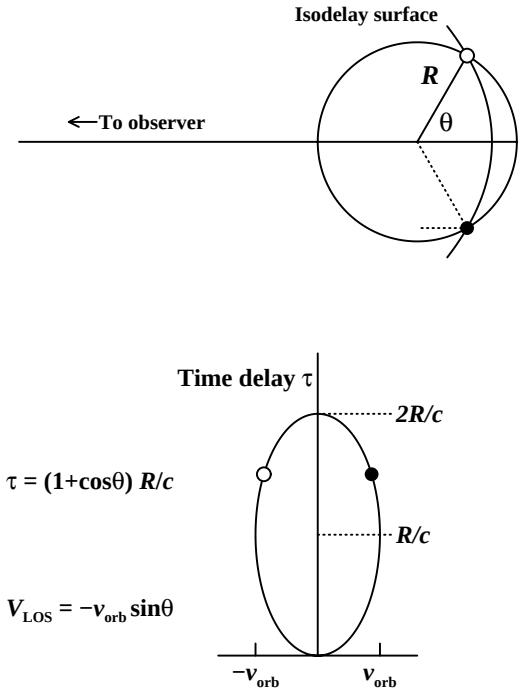

Fig. 2 Top: A notional BLR comprised of clouds orbiting the central source counterclockwise in a circular orbit of radius R. The dotted line shows (1) the path of an ionizing photon to a BLR cloud at coordinate $(R, -\theta)$ plus the path of an emission-line photon until it is as the same distance from the observer as the continuum source. The light travel time along the dotted path is $\tau = (1 + \cos\theta)R/c$, which is the time lag the observer sees between a continuum outburst and the response of the cloud. All points on the "isodelay surface" have the same delay relative to the continuum. Bottom: the same circular BLR projected into the observable quantities of Doppler velocity and time-delay; this is a very simple velocity–delay map.

At this point, an assumption about how the individual clouds re-emit line radiation can be intrduced. The simplest assumption is that the line emission is isotropic, i.e., $\Psi(\theta) = \epsilon$, a constant. To transform this to the observable velocity–time-delay coordinates,

$$\Psi(\tau)\, d\tau = \Psi(\theta) \frac{d\theta}{d\tau}\, d\tau. \tag{3}$$

From eq. (2).

$$\frac{d\tau}{d\theta} = -\frac{R}{c} \sin\theta. \tag{4}$$

It is simple to show then that

$$\Psi(\tau)\, d\tau = \frac{c\epsilon}{R\,(2c\tau/R)^{1/2}\,(1 - c\tau/2R)^{1/2}}\, d\tau \tag{5}$$

and that the mean response time for the ring is

$$\langle \tau \rangle = \frac{\int \tau \Psi(\tau)\, d\tau}{\int \Psi(\tau)\, d\tau} = \frac{R}{c}, \tag{6}$$

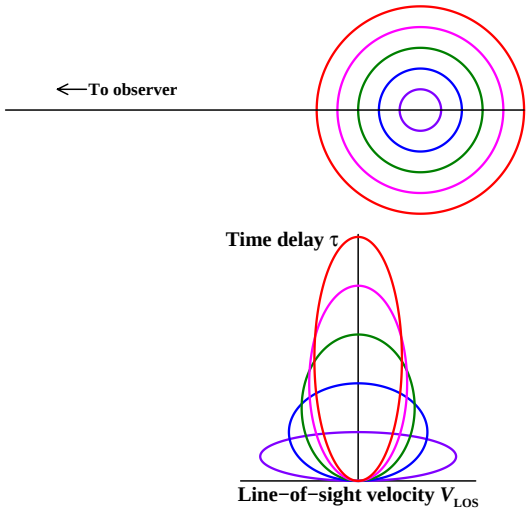

Fig. 3 Similar to Fig. 2, except for a series of rings in circular Keplerian orbits. Note in particular the "Keplerian taper" of the velocity–delay map at increasing time delay.

as is intuitively obvious. A more realistic assumption is that much of the line emission is directed back toward the ionizing source because the BLR clouds are very optically thick even in the lines. A simple parameterization is that $\Psi(\theta) = (1 + A\cos\theta)/2$. Isotropy is the case $A = 0$ and complete anisotropy (which is, incidentally, perhaps appropriate for Lyα λ1215) corresponds to $A = 1$ (Ferland et al. 1992).

Using a similar transformation for the case of isotropic re-emission, it is easy to show that

$$\Psi(V_{\rm LOS})\,dV_{\rm LOS} = \frac{\epsilon}{v_{\rm orb}\left(1 - V_{\rm LOS}^2/v_{\rm orb}^2\right)^{1/2}}\,dV_{\rm LOS}. \tag{7}$$

A useful measure of the line width is the line dispersion $\sigma_{\rm line}$; for a ring, the line dispersion is

$$\sigma_{\rm line} = \left(\langle V_{\rm LOS}^2\rangle - \langle V_{\rm LOS}\rangle^2\right)^{1/2} = \frac{v_{\rm orb}}{2^{1/2}}. \tag{8}$$

For comparison, for such a ring, FWHM $= 2v_{\rm orb}$.

A velocity–delay map for any other geometry and velocity field can be constructed similarly.

3.2.4 Reverberation Mapping Results: Velocity–Delay Maps

As noted above, both continuum and emission-line variations are usually not very large ($< 20\%$) on a reverberation timescale. This alone makes it very difficult to recover a velocity–delay map from spectrophotometric monitoring data. Indeed, the relative photometric accuracy must be extremely good: for ground-based spectra, for which absolute spectrophotometry at even the 5% level is notoriously difficult to achieve, this is usually accomplished by using the [O III] $\lambda\lambda$4959, 5007 narrow lines as an internal flux calibrator. These lines arise in the spatially extended low-density narrow-line region, so both the light-travel time and recombination time are sufficiently long to ensure that

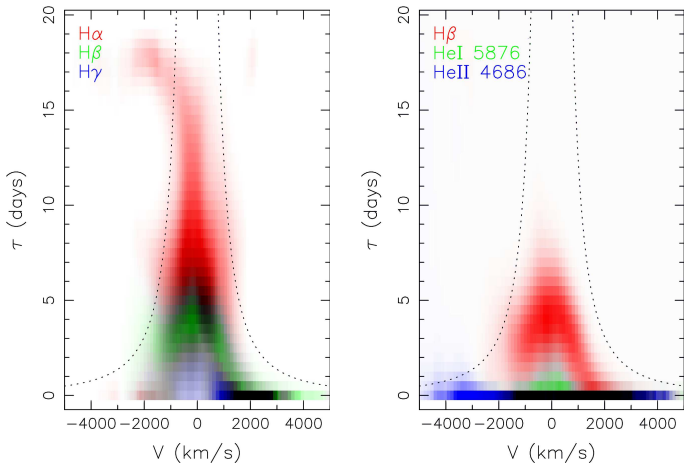

Fig. 4 Left: Velocity–delay maps for the Balmer lines in Arp 151. Note the clear inflow signature for time delays above 15 light days. Right: Velocity–delay maps for Hβ, He I λ5876, and He II λ4686 in Arp 151. Bentz et al. (2010b).

the flux in these lines is constant on reverberation timescales. An alternative calibration strategy is to rotate the spectrograph slit to a position where a nearby non-variable star can be observed simultaneously. An even better strategy that is gaining popularity is to use simultaneous imaging data to define the continuum light curve and calibrate the spectra.

Time sampling is critical (Horne et al. 2004). As a rule of thumb the duration of the monitoring campaign has to be at least ~ 3 times the longest timescale of interest ($2R/c$) for an accurate measurement of the mean response time and rather longer than this to recover a velocity–delay map. The sampling rate ultimately tranforms into the spatial resolution of the velocity–delay map and thus needs to be high.

When reverberation studies began in earnest in the late 1980s, most programs were designed with the modest goal of measuring mean response times for various emission lines and characterizing the variability characteristics of AGNs as a function of luminosity, as discussed in §3.2.5 below. There were early attempts to recover velocity–delay maps (e.g., Ulrich & Horne 1996; Wanders et al. 1997; Kollatschny 2003a); these revealed some structure, but little detail. It is only relatively recently that reliable velocity–delay maps have begun to appear in the literature (Bentz et al. 2010b; Grier et al. 2013), with examples shown in Figures 4 and 5. To provide some insight into interpreting these maps, Figure 6 shows examples of velocity–delay maps for some simple "toy models;" these demonstrate how inflow models (spherical infall, in the top two panels of Figure 6) are characterized by the earlier response of the red wing of the line (closer to us, but receding) followed by the response of the blue side of the line (farther away for us and approaching). BLRs in which the cloud motions are in Keplerian orbits, either in a disk as in the lower left of Figure 6 or in a spherical shell as in the lower right, have symmetric structures that show a characteristic Keplerian "taper:" all the gas with large line-of-sight velocities is at small lags, close to the continuum source, and at large lags, only small values of $V_{\rm LOS}$ are observed.

The velocity–delay maps for Arp 151 in Figure 4 strongly suggest a disk-like structure, and the Balmer lines hint at an infall component (in the Balmer lines at time

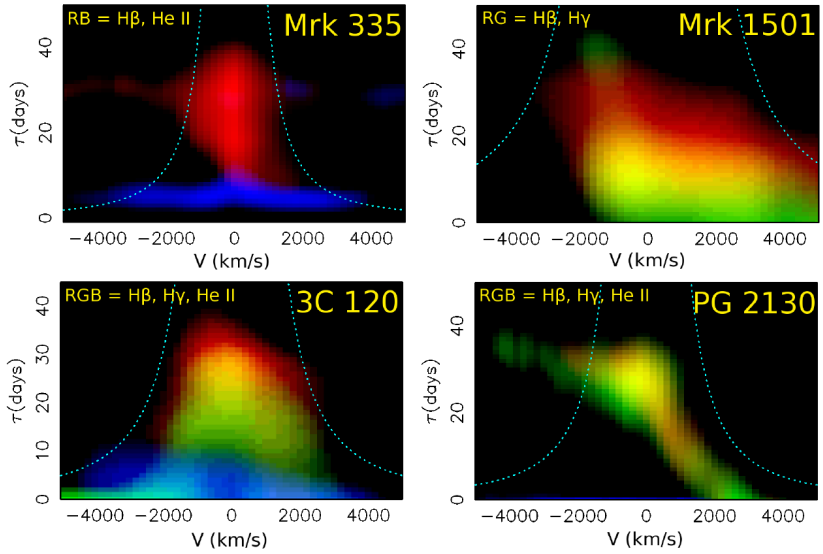

Fig. 5 Velocity–delay maps for four AGNs. 3C 120 has a disk-like structure and evidence for infall is apparent in each of these. Grier et al. (2013).

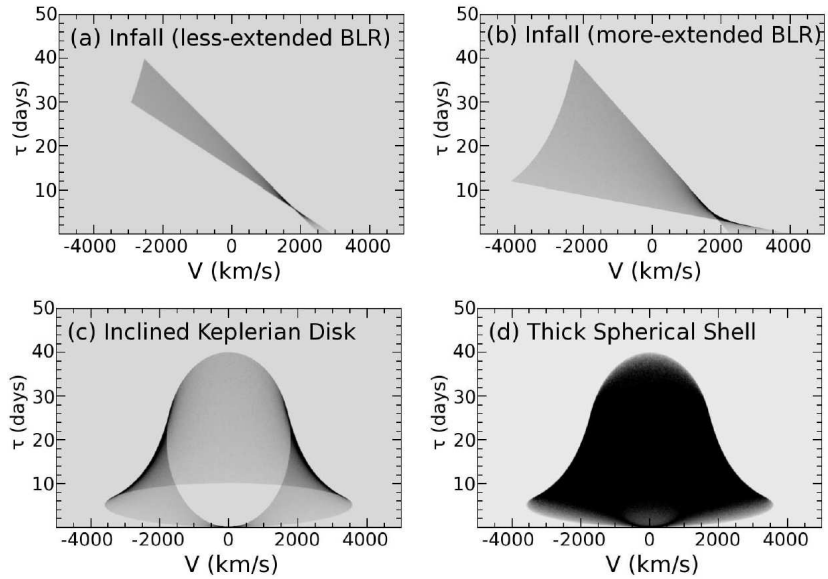

Fig. 6 Toy models of velocity–delay maps for spherical infall (top two panels) and a Keplerian disk (lower left) and a thick shell of randomly inclined circular Keplerian orbits (lower right). Grier et al. (2013).

delays larger than ~ 15 days) and possibly a localized hot spot in the BLR disk (based on the enhanced emission at velocity–delay coordinates ($+2000\,\mathrm{km\,s^{-1}}$, 0 days). More detailed modeling by Brewer et al. (2011) based on formalism developed by Pancoast, Brewer, & Treu (2011) favors a thick disk-like BLR geometry at an inclination[3] of $\sim 22^{\,\mathrm{o}}$, with infall favored, and a value for the central mass $M_{\rm BH} = 3.2\,(\pm 2.1)\times 10^6\,M_\odot$.

The velocity–delay maps in Figure 5 are so recent that detailed physical modeling has not yet been done. Some of these strongly hint at a disk-like geometry (e.g., 3C 120) and in each case there is evidence for infall.

3.2.5 Reverberation Mapping Results: Lags

As already noted, the primary goal of most reverberation monitoring campaigns that have been undertaken to date has been to determine the mean response time of the integrated emission line, i.e., to measure the "lag" between continuum and emission-line variations. The most up-to-date methodology for making these measurements is that described by Zu, Kochanek, & Peterson (2011).

The first high-sampling rate multiwavelength reverberation monitoring program was undertaken in 1988–89 by the International AGN Watch (Clavel et al. 1991; Peterson et al. 1991; Maoz et al. 1993; Dietrich et al. 1993; Alloin et al. 1994). Since then, emission-line lags have been measured for about 50 AGNs, mostly for the Hβ emission line, and for multiple emission lines in only a few cases. Peterson et al. (2004) provide a homogeneous compilation of most of the high-quality reverberation results available as of a decade ago. More recent large-scale campaigns have been undertaken by the Lick AGN Monitoring Program (LAMP), described by Bentz et al. (2009c), Barth et al. (2011a), and Barth et al. (2011b), by a consortium of astronomers primarily in eastern Europe, Mexico, and Germany (e.g., Shapovalova et al. 2010; Popović et al. 2011; Shapovalova et al. 2012) and by the author's group of collaborators (Bentz et al. 2006b; Denney et al. 2006; Bentz et al. 2007; Denney et al. 2010; Grier et al. 2012b). Programs to measure the C IV λ1549 lag in a very low-luminosity AGN (Peterson et al. 2005) and a very high-luminosity AGN (Kaspi et al. 2007) have also been reported. All of these efforts are continuing, and new results appear regularly.

These studies have led to several important findings:

- Within a given AGN, the higher-ionization lines have smaller lags than the lower-ionization lags, demonstrating ionization stratification of the BLR. This also shows that the BLR gas is distributed over a range of radii from the central source, and the lag for a particular emission line represents the radius at which the combination of emissivity and responsivity is optimized for that particular emission line.
- The variable part of the emission line can be isolated by constructing the rms residual spectrum from all monitoring data. In the rms residual spectrum, the higher ionization lines are broader than the low ionization lines, in such a way that the the product $\Delta V^2\tau$ is constant within a given source, suggesting that the BLR is virialized.
- There is a relationship between the size of the BLR R and the AGN luminosity L of the approximate form $R \propto L^{1/2}$.

[3] Brewer et al. (2011) define the inclination angle to be the complement of the usual astronomical convention where $i = 0$ is face-on. The value given here is corrected to the standard astronomical convention.

These results underpin our efforts to measure the masses of the central sources in these objects, as discussed in the next session.

4 Reverberation-Based Black Hole Masses

4.1 Virial Mass Estimates

For every AGN for which emission-line lags and line widths have been measured, consistency with the "virial relationship" is found (Peterson & Wandel 1999, 2000; Kollatschny 2003a; Peterson et al. 2004; Bentz et al. 2010a). This also appears to be true when the lag and line width are measured for the same emission line when the AGN is in very different luminosity states. This strongly suggests that the BLR dynamics are dominated by the central mass, which is then

$$M_{\rm BH} = f\left(\frac{\Delta V^2 R}{G}\right), \tag{9}$$

where ΔV is the line width and R is the reverberation radius $c\tau$. The quantity in parentheses that contains the two directly observable parameters has units of mass and is sometimes referred to as the "virial product." The effects of everything unknown — the BLR geometry, kinematics, and inclination — are then subsumed into the dimensionless factor f, which will be different for each AGN, but is expected to be of order unity. Presumably, individual values of f can be determined if there is some other way of determining the black hole mass. In the absence of a second direct measurement, it has been common practice to use the $M_{\rm BH}$–σ_* relationship for this purpose. The relationship between central black hole mass and bulge velocity dispersion that is seen in quiescent galaxies (Gebhardt et al. 2000a; Ferrarese & Merritt 2000) is also seen in AGNs (Gebhardt et al. 2000b; Ferrarese et al. 2001; Nelson et al. 2004) although of course, the host-galaxy velocity dispersions are are much more difficult to measure in AGNs because of the bright active nucleus and because even the nearest AGNs are typically quite distant (Dasyra et al. 2007; Watson et al. 2008). By assuming that the $M_{\rm BH}$–σ_* relationship is the same in quiescent and active galaxies, it becomes possible to compute a mean value for the scaling factor, which turns out to be $\langle f \rangle \sim 5$ (Onken et al. 2004; Woo et al. 2010; Park et al. 2012), although it is noted that Graham et al. (2011) argue that in practice this process has been oversimplified. Figure 7 shows the $M_{\rm BH}$–σ_* relationship for quiescent galaxies and AGNs using the assumption that $\langle f \rangle = 5.25$. The scatter around this relationship amounts to about ~ 0.4 dex, which is a reasonable estimate of the accuracy of the "virial method" of estimating black hole masses.

Sometimes concern is expressed that the empirical value of $\langle f \rangle$ seems uncomfortably large for a truly virialized system. However, it must be kept in mind that AGN unification stipulates that Type 1 AGNs are generally observed at low values of inclination, much closer to face-on than edge-on. Actually, the fact that $\langle f \rangle$ is as *small* as it is tells us that the BLR must have a fairly significant velocity component in the polar direction; it is surely not a flat disk.

To return to a point made earlier, reverberation mapping is a *direct* measure of black hole mass, but it is a *secondary* method because, at the present time, it relies on an independent method, the $M_{\rm BH}$–σ_* relationship, to calibrate the mass scale through determination of $\langle f \rangle$.

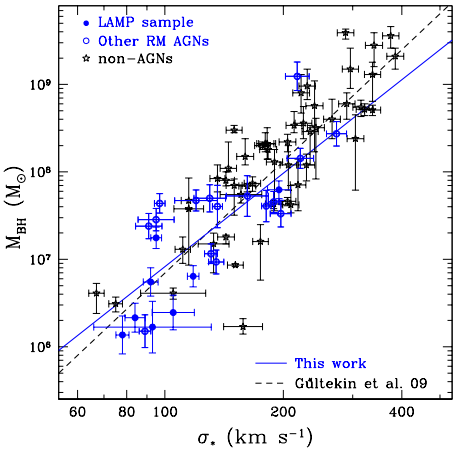

Fig. 7 The $M_{\rm BH}$–σ_* relationship. Quiescent galaxies are shown in black and AGNs are shown in blue. Woo et al. (2010).

4.2 Testing Reverberation-Based Masses

In addition to the virial relationship $\Delta V \propto R^{-1/2}$ seen in the broad emission lines and the similarity of the $M_{\rm BH}$–σ_* relationships for active and quiescent galaxies, there is other evidence that supports the general veracity of reverberation-based masses:

- The well-known correlation between central black hole mass and host-galaxy bulge luminosity (Kormendy & Richstone 1995; Magorrian et al. 1998) is also seen in active galaxies (Bentz et al. 2009a). There is very good agreement between these when the AGN black hole masses are calibrated by using the $M_{\rm BH}$–σ_* relationship.
- In a small number of nearby AGNs, it is possible to measure or at least constrain the black hole mass using more than one direct method of mass measurement, as shown in Table 1. To within the factor of two or three uncertainties in each of these methods[4] (except for megamasers), the multiple measurements are in generally good agreement. Table 1 also underscores the important point that reverberation mapping and megamasers motions cannot be used in the same source: the former can be employed in Type 1 AGNs and the latter are likely to be found only in Type 2 AGNs.
- It was noted in §3.2.4 that the black hole mass is a free parameter in modeling velocity–delay maps. So far detailed modeling has been done in only two cases, Arp 151 (Brewer et al. 2011) and Mrk 50 (Pancoast et al. 2012). In both cases, the masses obtained from modeling are in reassuringly good agreement with those based on eq. (9) using the nominal value $f = 5.25$.

In closing this section, it is noted that an unresolved issue is whether or not radiation pressure plays a sufficiently important role in the BLR dynamics that it affects black hole mass measurement (Marconi et al. 2008; Netzer & Marziani 2010). Since radiation pressure is a $1/r^2$ force, it is not easily distinguished from gravity: ignor-

[4] Note that the errors quoted in Table 1 are statistical. Systematic errors have not been included.

Table 1 Comparison of Black Hole Mass Measurements

Method	**NGC 4258**	**NGC 3227**	**NGC 4151**
	(Units $10^6\ M_\odot$)		
Direct methods:			
Megamasers	38.2 ± 0.1[1]	N/A	N/A
Stellar dynamics	33 ± 2[2]	7–20[3]	≤ 70[4]
Gas dynamics	25–260[5]	20^{+10}_{-4} [6]	$30^{+7.5}_{-22}$ [6]
Reverberation	N/A	$7.63^{+1.62}_{-1.72}$ [7]	46 ± 5[8]
Indirect methods:			
$M_{\rm BH}$–σ_*[9]	13	25.0	6.1
R–L scaling[10]	N/A	15	65

[1]Herrnstein et al. (2005). [2]Siopsis et al. (2009). [3]Davies et al. (2006). [4]Onken et al. (2007). [5]Pastorini et al. (2007). [6]Hicks & Malkan (2008). [7]Denney et al. (2010). [8]Bentz et al. (2006b). [9]Gültekin et al. (2009). [10]McGill et al. (2008).

ing radiation pressure simply leads to systematic underestimation of AGN black hole masses.

5 Indirect Masses Estimates Anchored by Reverberation Results

As noted earlier, the distinct advantage of reverberation mapping compared to other methods of measuring the masses of supermassive black holes in galaxies is that it substitutes time resolution for angular resolution. In principle, it can be used to measure the masses of black holes even in the most distant quasars. It does, however, have the corresponding disadvantage of being resource-intensive: a reliable reverberation measurement requires a large number of observations, typically 30–50 at minimum. This drives a search for shortcuts that will allow mass estimates from simpler or fewer observations. Fortunately, and remarkably, reverberation mapping provides a suitable scaling relationship that allows estimation of AGN black hole masses from single spectra.

5.1 The Radius–Luminoisty Relationship

In §3.2.5, it was noted that reverberation mapping has revealed an empirical relationship between the radius of the BLR and the luminosity of the AGN. This was not in any way unexpected. Prior to the advent of reverberation mapping, the principal means of studying the BLR was through photoionization equilibrium modeling (e.g., Ferland & Mushotzky 1982), where one tries to adjust the model parameters to produce relative emission-line intensities that match the observations. Photoionization equilibrium models are characterized by the shape of the ionizing continuum that irradiates the emission-line clouds, the chemical composition of the gas, and an ionization parameter U that is the ratio of the ionizing photon density to the particle density at the irradiated face of the clouds,

$$U = \frac{Q(H)}{4\pi R^2 n_{\rm e} c}, \tag{10}$$

where $n_{\rm e}$ is the particle density and $Q(H)$ is the rate at which hydrogen-ionizing photons are produced by the central source, which is at a distance R from the emission-line

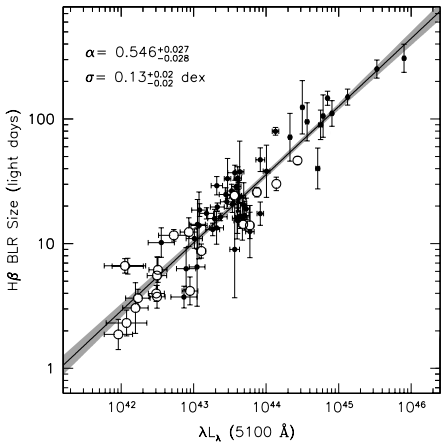

Fig. 8 The R–L relationship between the size of the BLR measured by the broad Hβ response as a function of the host-corrected AGN luminosity. Open circles are new or improved data since Bentz et al. (2009b). Bentz et al. (2013).

clouds. The similarity of AGN spectra over many orders of magnitude in luminosity (e.g., Dietrich et al. 1993; Vanden Berk et al. 2004) suggests that U and $n_{\rm e}$ are approximately the same for all AGNs. By assuming that $L \propto Q(H)$,

$$R \propto L^{1/2}. \tag{11}$$

The great utility of the ionization parameter formulation was first recognized by Davidson (1972), although he is not often credited with this insight, possibly because instead of expressing U in terms of L and R, he used the ionizing flux $F = L/4\pi R^2$, so the distance did not appear explicitly.

Thus from the beginning of reverberation investigations, a relationship like equation (11) was expected, and it was searched for even with the first marginally sampled and undersampled reverberation data (e.g., Koratkar & Gaskell 1991; Peterson 1993). The first observationally well-defined version of the R–L relationship was by Kaspi et al. (2000), who found $R \propto L^{0.7}$. A refinement of the database led to a somewhat shallower slope (Kaspi et al. 2005), but it was only when contamination of the luminosity by host-galaxy starlight was accounted for (Bentz et al. 2006a, 2009b, 2013) that the slope was close to the naïve photoionization prediction. The most recent version of the R–L relationship for the broad Hβ emission line and the optical continuum is shown in Figure 8. It is also worth noting that the existence of the R–L relationship has been confirmed independently by gravitational microlensing studies (Guerras et al. 2013).

While the existence of the R–L relationship is not surprising, the tightness of the relationship is. The intrinsic scatter in the relationship seems to be ~ 0.13 dex (Figure 8). Typical *good* individual reverberation lag measurements are accurate to about 0.09 dex, so, at least for Hβ, the R–L relationship does almost as well as an actual reverberation measurement, provided one has an accurate host-corrected AGN luminosity.

Unfortunately, Hβ is the *only* emission line for which the R–L relationship is empirically well-calibrated. There are, however, a limited number observations that seem to

indicate that a relationship similar to that between $H\beta$ and the AGN optical continuum holds for C IV λ1549 and the UV continuum as well (Kaspi et al. 2007).

5.2 Indirect Masses from R–L

The great utility of equation (11) is that it provides a quick way to estimate the BLR size and thus black hole mass from a single spectrum, limited only by the accuracy of the flux calibration and the starlight removal. Of course, since many AGN luminosity measures are highly correlated, it is entirely possible to use other, sometimes easier-to-measure, luminosities — e.g., X-ray, broad Balmer and Paschen lines, narrow [O III] λ5007, narrow [O IV] λ25.8 μm (Wu et al. 2004; Greene et al. 2010; Landt et al. 2011) — as surrogates for the host-corrected optical luminosity, although none of these is yet very well calibrated.

The first attempts to use the R–L relationship in an informed way to estimate masses (variously called the "photoionization method" or "single-epoch spectrum method") were by Laor (1998) and Wandel, Peterson, & Malkan (1999), in both cases using the broad Hβ line. This was subsequently extended to the UV emission lines Mg II λ2798 and C IV λ1549 (McLure & Jarvis 2002; Vestergaard 2002, 2004; Vestergaard & Peterson 2006; Kollmeier et al. 2006) to allow applications at higher redshift.

For the sake of completeness, indirect measures of black hole mass are included in the bottom two lines of Table 1. These underscore the fact that indirect mass estimates are no more accurate than a factor of several. The principal value of the indirect methods is to produce large samples of mass estimates that are statistically, rather than individually, accurate.

5.3 Problems with Indirect Mass Measurements

The first thing one needs to keep in mind that at the present time there is no consensus on the exact prescription one needs to follow to compute a black hole mass from a single spectrum of a quasar. This is a field that is still in a developmental stage.

Something that is generally not appreciated is that estimating the BLR size from the R–L relationship is the easy part (again assuming that L is determined accurately). The more ambiguous part is characterizing the line widths. In §3.2.5, it was noted that in determining a reverberation-based mass it is most common to use the line widths measured in the rms residual spectrum, which isolates the part of the emission line that is actually varying, and to characterize the line width by the line dispersion (second moment) of the profile. Characterizing the line width in "single-epoch" spectra presents some problems:

– The spectrum contains contaminating features that do not appear in the rms residual spectrum. The narrow-line components of the broad emission lines and the constant host-galaxy continuum disappear in the rms residual spectrum; in a "single-epoch" or mean spectrum, they need to be modeled out. In the vicinity of Hβ, there are also blended Fe II features — these vary slowly, but do not appear to "reverberate" as cleanly as other broad lines (Vestergaard & Peterson 2005; Kuehn et al. 2008), so they are usually not seen the rms residual spectra. In the case of the

C IV λ1549, He II λ1640, O III] λ1663 complex there is an unidentified emission feature at ~ 1600 Å that is problematic (Fine et al. 2010). Mg II λ2798 is also difficult because of contamination by broad blends of Fe II.

- There are intrinsic differences between the widths of certain emission lines in mean (or single-epoch) and rms residual spectra. As an example, Ferland, Korista, & Peterson (1990) find that the far wings of Hβ do not vary in Mrk 590 and suggest that this might be because the highest velocity BLR gas, presumably closest to the continuum source, is optically thin in the ionizing continuum. As another example, Denney (2012) finds dramatic differences in the C IV λ1549 profiles between mean and rms residual spectra, but that these are correlated with the emission-line profile. In general, it seems that it should be possible to one way or another calibrate out the differences between mean and rms residual spectra.
- The most common, and intended, use of indirect methods is for surveys. Survey spectra, however, are generally quite noisy, typically below a threshold where there are not systematic errors of various type introduced by low signal-to-noise ratio (S/N) (Denney et al. 2009). Again, in principle, these effects are statistically correctable.

There are two other continuing problems in determining masses.

- Many studies continue to use FWHM to characterize the line widths. This is, of course, a very tempting thing to do because FWHM is generally easily measured and less affected by blending than the line dispersion $\sigma_{\rm line}$. However, the reverberation masses are calibrated using $\sigma_{\rm line}$, not FWHM. This actually matters a great deal because the ratio FWHM/$\sigma_{\rm line}$ is *a strong function of line width*, as shown in Figure 9.
- A related problem is that many studies, particulary those based on lower S/N survey data, fit single Gaussians to the emission lines. For a Gaussian, as is well known, FWHM/$\sigma_{\rm line} \approx 2.35$ which, as can be seen in Figure 9 is *on average* not a bad approximation for a quasar emission line, but it is terrible at both the high-width and low-width ends of the distribution. The problem again is that *the line profile is a strong function of line width.*

The impact of using FWHM rather than $\sigma_{\rm line}$ is, at fixed luminosity L (or, equivalently, BLR radius R), to stretch out the distribution in mass, overestimating the highest masses (with the broadest lines) and underestimating the lowest masses (with the narrowest lines). This introduces a bias into the mass functions derived from these measurements. Of course, it is possible to remove this bias through the clear relationship between $\sigma_{\rm line}$ and FWHM shown in Figure 9; in principle, $\sigma_{\rm line}$ can be inferred, with some loss of precision, from FWHM.

A fair question to ask at this point is why not use FWHM to characterize the line widths in the original reverberation data instead of $\sigma_{\rm line}$? There are a number of reasons for preferring $\sigma_{\rm line}$ over FWHM as the line-width measure:

1. Multiple reverberation measurements of the same source should always yield the same mass. NGC 5548 is our ideal test case here, as there are over a dozen reverberation measurements of the lag and line width for Hβ alone, with lags ranging from a few days to nearly a month. For these measurements, $\sigma_{\rm line}$ yields a more consistent mass than does FWHM.
2. For AGNs in which multiple emission lines have been measured, the virial relationship is tighter for $\sigma_{\rm line}$ than for FWHM (Peterson et al. 2004). This is essentially the same test as above.

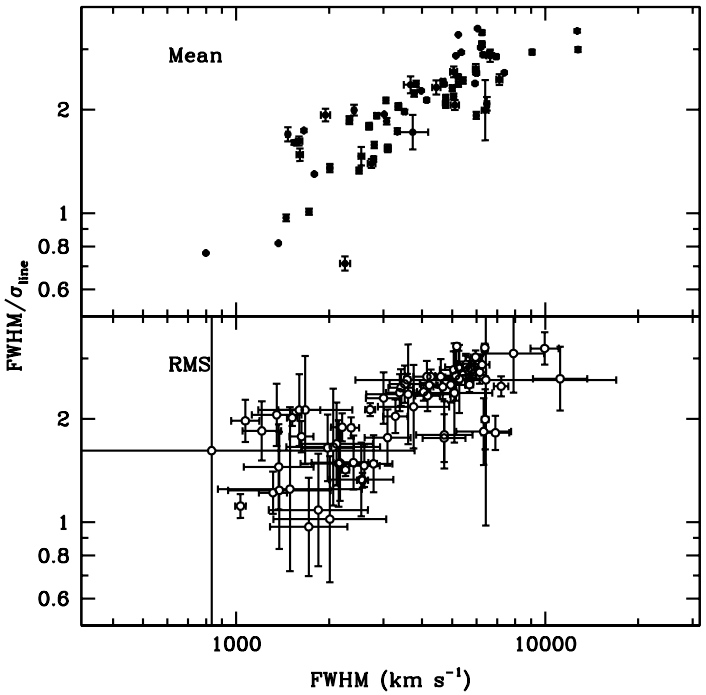

Fig. 9 Ratio of two measures of the emission line width for Hβ in reverberation-mapped AGNs, full-width at half maximum (FWHM) and line dispersion $\sigma_{\rm line}$ as a function of line width for the compilation of Peterson et al. (2004). Top panel is for mean spectra, bottom panel is for rms residual spectra. Values in top panel are very approximate since no deblending of contaminants (except narrow emission components) was undertaken.

3. Steinhardt & Elvis (2010) find that when they plot AGN luminosity as a function of black hole mass for individual redshift bins, the quasars at the high-mass end of the bin fall farther and farther below the Eddington limit, an effect they refer to as the "sub-Eddington boundary." This is, in fact, exactly the bias that would be expected by using FWHM (and/or Gaussian fits) instead of $\sigma_{\rm line}$, which was indeed the case for the line-width measurements used in this study (Shen et al. 2008); the highest masses are overestimated and the lowest masses are underestimated, which would appear to rotate a distribution parallel to the Eddington limit (i.e., at fixed Eddington rate) to something shallower. Rafiee & Hall (2011) measured $\sigma_{\rm line}$ directly from the line profiles for essentially the same sample of AGNs and the "sub-Eddington boundary" effect either vanishes or is greatly reduced.

None of these arguments is iron-clad (e.g., the sub-Eddington boundary could be real), but they certainly indicate that a more critical examination of how to characterize line widths deserves consideration.

6 Alternative Paths to Black Hole Masses

There are other methods of black hole mass measurement that are used less frequently, either because they require special cirumstances are or lead to lower-confidence estimates of black hole mass.

- The black hole mass can be measured from the gravitational redshift of the broad emission lines. While the BLR, at several hundred gravitational radii from the black hole, is far enough that relativistic effects can usually be ignored, the gravitional redshift
$$c\Delta z = \frac{GM_{\rm BH}}{cR_{\rm BLR}}, \tag{12}$$
can be of order 100 $\mathrm{km\,s^{-1}}$ for many of the reverberation-mapped AGNs and is therefore detectable at sufficiently high spectral resolution. A very credible detection has been reported by Kollatschny (2003b).
- The temperature structure of an accretion disk depends on the mass and mass accretion rate. It is therefore possible to obtain the mass of the black hole by fitting the observed continuum with an accretion disk model. While this is notoriously difficult, some current models (Gliozzi et al. 2011) yield masses that seem to be in reasonable agreement with reverberation-based masses.
- X-ray observations have in some cases been used to estimate black hole masses. For example, Iwasawa, Miniutti, & Fabian (2004) estimate a black hole mass by associating modulations of the X-ray Fe Kα emission line with orbital motion of an accretion disk. In another case, a reverberation lag between the directly emitted X-ray continuum and its reflection off the accretion disk has also been used to estimate the mass of the central black hole in an AGN (Fabian et al. 2009).
- X-ray observations also reveal that the power spectral density function of accreting black holes shows a characteristic "break frequency," becoming much steeper at high frequency (Markowitz et al. 2003; Papadakis 2004; McHardy et al. 2006). The break frequency is a function of both mass and mass accretion rate and can be used to estimate these quantities. The origin of the break is not well-understood, although it has been suggested recently that it is associated with the cooling timescale for Comptonization of electrons (Ishibashi & Courvoisier 2012).
- By assuming that X-ray warm absorbers in AGNs are radiatively accelerated, an upper limit on the central black hole mass can be calculated (Morales & Fabian 2002). Given the model uncertainties, these are in surprisingly good agreement with the reverberation measurements.

7 The Future

In addition to trying to capture the current state of the art, a review article should also attempt to identify particularly important directions that might be undertaken in the future. Based on this discussion, here are a few investigations that might be pursued to improve measurement of the masses of black holes in AGNs:

- **Velocity–delay maps for high-ionization lines.** As discussed in §3.2.4, the Balmer lines are emitted by lower-ionization gas that seems to be infalling and at least sometimes in a disk-like structure. Absorption-line studies suggest, by contrast, that the strong high-ionization lines in the UV arise in outflows. A complete

picture of gas flows in active nuclei will therefore require contemporaneous velocity–delay maps for both high-ionization and low-ionization lines.
- **Modeling BLR kinematics.** Velocity–delay maps provide entirely new constraints that should allow tremendous improvements in forward modeling of the BLR and, consequently, determination of the masses of the central black holes.
- **The radius–luminosity relationship at high luminosity.** This is especially important for the C IV line because of the potential importance of this line in determining black hole masses at high redshift. Even the Hβ R–L relationship is sparsely populated at high luminosity (Figure 8) and by sources for which the light curves are not exceptionally well-sampled. It is important to quantify the systematic effects and intrinsic scatter because of the potential importance of using this relationship for cosmological applications (e.g., Watson et al. 2011).
- **Characterization of line widths.** At the present time, there is no consensus "best practice" for characterization of broad emission-line widths for black hole mass determination. How this is done for single-epoch spectra is even more controversial and, indeed, the case that C IV in particular can be used to estimate black hole masses with any confidence at all needs to be made.
- **Direct comparisons of methods of mass measurement.** The opportunities for this are limited, of course, by the necessity of resolving $R_{\rm BH}$ (§1) to relatively nearby systems. As the precison of mass measurement improves, even in the immediately foreseeable future the efficacy of the comparisons will be limited by uncertainties in the distances to the nearest AGNs on account of their peculiar motions relative to the Hubble flow (Bentz et al. 2013). Obtaining accurate distances to the nearst AGNs is a matter of sone urgency since it will get a lot harder following the inevitable retirement of *Hubble Space Telescope*.
- **Expanding the reverberation-mapped population.** The sample of some 50 or so AGNs that have been the targets of reverberation-mapping programs is certainly plagued by selection effects: for the most part, the AGNs that have been the targets of reverberation monitoring campaigns have been selected by some combination of their apparent brightness, known variability, or favorable position in the sky. Richards et al. (2011) note, for example, the absence in the reverberation sample of quasars with blueshifted C IV emission. This is, of course, not surprising given because such objects are found at high redshift and the reverberation sample is mostly at $z < 0.2$. Certainly this is an area of concern that must be addressed in the future.

Acknowledgements The author is grateful for support by the US National Science Foundation through grant AST-1008882 to The Ohio State University and for the kind hospitality of the International Space Science Institute in Bern, where this work was first presented. The author thanks Misty Bentz for providing Figures 4 and 8, Kate Grier for Figures 1, 5 and 6, and Jong-Hak Woo for Figure 7.

References

D. Alloin, J. Clavel, B.M. Peterson, G.A. Reichert, & G.M Stirpe, in *Frontiers of Space and Ground-Based Astronomy: The Astrophysics of the 21st Century*, ed. W. Wamsteker, M.S. Longair, & Y. Kondo (Dordrecht, Kluwer, 1994).
Y. Andrillat & S. Souffrin, Astrophys. Letters, **1**, 111 (1968).
R.R.J. Antonucci & R.D. Cohen, Astrophys. J., **271**, 564 (1983).
J.N. Bahcall, B.Z. Kozlovsky, & E.E. Salpeter, Astrophys. J., **171**, 467 (1972).

A.J. Barth et al., Astrophys. J., **732**:121 (2011a).
A.J. Barth et al., Astrophys. J., **743**:L4 (2011b).
M.C. Bentz, B.M. Peterson, R.W. Pogge, M. Vestergaard, & C.A. Onken Astrophys. J., **644**, 133 (2006a).
M.C. Bentz, B.M. Peterson, R.W. Pogge, & M. Vestergaard, Astrophys. J., **694**, L166 (2009a).
M.C. Bentz, B.M. Peterson, H. Netzer, R.W. Pogge, & M. Vestergaard, Astrophys. J., **697**, 160 (2009b).
M.C. Bentz et al., Astrophys. J., **651**, 775 (2006b).
M.C. Bentz et al., Astrophys. J., **662**, 205 (2007).
M.C. Bentz et al., Astrophys. J., **705**, 199 (2009c).
M.C. Bentz et al., Astrophys. J., **716**, 993 (2010a).
M.C. Bentz et al., Astrophys. J., **720**, L46 (2010b).
M.C. Bentz et al., submitted to Astrophys. J.(2013).
R.D. Blandford & C.F. McKee, Astrophys. J., **255**, 419 (1982).
G. Bower et al., Astrophys. J., **492**, L111 (1998).
B.J. Brewer et al., Astrophys. J., **733**:L33 (2011).
E.M. Burbidge, ARAA, **5**, 399 (1967).
J. Clavel et al., Astrophys. J., **366**, 64 (1991).
S. Collin-Souffrin, D. Alloin, & Y. Andrillat, Astron. Astrophys., **22**, 343 (1973).
N. Cretton, P.T. de Zeeuw, R.P. van der Marel, & H.-W. Rix, Astrophys. J. Suppl., **124**, 383 (1999).
E. Dalla Bontà, L. Ferrarese, E.M. Corsini, J. Miralde Escudé, L. Coccato, M. Sarzi, A. Pizzella, & A. Beifiori, Astrophys. J., **690**, 537 (2009).
K. Davidson, Astrophys. J., **171**, 213 (1972).
R.I. Davies et al., Astrophys. J., **646**, 754 (2006).
G. de Francisco, A. Capetti, & A. Marconi, Astron. Astrophys., **479**, 355 (2008).
K.M. Dasyra, L.J. Tacconi, R.I. Davies, R. Genzel, D. Lutz, B.M. Peterson, S. Veilleux, A.J. Baker, M. Schweitzer, & E. Sturm, Astrophys. J., **657**, 102 (2007).
K.D. Denney, Astrophys. J., **759**:44 (2012).
K.D. Denney, B.M. Peterson, M. Dietrich, M. Vestergaard, & M.C. Bentz, Astrophys. J., **692**, 246 (2009).
K.D. Denney et al., Astrophys. J., **653**, 152 (2006).
K.D. Denney et al., Astrophys. J., **721**, 715 (2010).
M. Dietrich et al., Astrophys. J., **408**, 146 (1993).
M. Dietrich, F. Hamann, J.C. Shields, A. Constantin, M. Vestergaard, F. Chaffee, C.B. Foltz, & V.T. Junkkarinen, Astrophys. J., **581**, 912 (2002).
A.C. Fabian et al., Nature, **459**, 540 (2009).
G.J. Ferland, K.T. Korista, & B.M. Peterson, Astrophys. J., **363**, L21 (1990).
G.J. Ferland & R.F. Mushotzky, Astrophys. J., **262**, 564 (1982).
G.J. Ferland, B.M. Peterson, K. Horne, W.F. Welsh, & S.N. Nahar, Astrophys. J., **387**, 95 (1992).
L. Ferrarese & H. Ford, Space Science Reviews, **116**, 523 (2005).
L. Ferrarese & D. Merritt, Astrophys. J., **539**, L9 (2000).
L. Ferrarese, R.W. Pogge, B.M. Peterson, D. Merritt, A. Wandel, & C.L. Joseph, Astrophys. J., **555**, L79 (2001).
S. Fine, S.M. Croom, J. Bland-Hawthorn, K.A. Pimbblet, N.P. Ross, D.P. Schneider, & T. Shanks, MNRAS, **409**, 591 (2010).
K. Gebhardt et al., Astrophys. J., **539**, L13 (2000a).
K. Gebhardt et al., Astrophys. J., **543**, L5 (2000b).
K. Gebhardt et al., Astrophys. J., **583**, 92 (2003).
R. Genzel, F. Eisenhauer, & S. Gillessen, Rev. Mod. Phys. **82**, 3121 (2010).
M. Gliozzi, L. Titarchuk, S. Satyapal, D. Prince, & I. Jang, Astrophys. J., **735**:16 (2011).
A.W. Graham, C.A. Onken, E. Athanassoula, & F. Combes, MNRAS, **412**, 2211 (2011).
J.E. Greene et al., Astrophys. J., **723**, 409 (2010).
C.J. Grier et al., Astrophys. J., **744**:L4 (2012a).
C.J. Grier et al., Astrophys. J., **755**:60 (2012b).
C.J. Grier et al., Astrophys. J., **764**:47 (2013).
E. Guerras, E. Mediavilla, J. Jimenez-Vicente, C.S. Kochanek, J.A. Muñoz, E. Falco, & V. Motta, Astrophys. J., in press [arXiv:1207.2042] (2013).
K. Gültekin et al., Astrophys. J., **698**, 198 (2009).

J.R. Herrnstein, J.M. Moran, L.J. Greenhill, & A.S. Trotter, Astrophys. J., **629**, 719 (2005).
E.K.S. Hicks & M.A. Malkan, Astrophys. J. Suppl., **174**, 31 (2008).
K. Horne, B.M. Peterson, S.J. Collier, & H. Netzer, PASP, **116**, 465 (2004).
W. Ishibashi & T.J.-L. Courvoisier, Astron. Astrophys., **540**, L2 (2012).
K. Iwasawa, G. Miniutti, & A.C. Fabian, MNRAS, **355**, 1073 (2004).
S. Kaspi, W.N. Brandt, D. Maoz, H. Netzer, D.P. Schneider, O. Shemmer, Astrophys. J., **659**, 997 (2007).
S. Kaspi, D. Maoz, H. Netzer, B.M. Peterson, M. Vestergaard, & B.T. Jannuzi, Astrophys. J., **629**, 61 (2005).
S. Kaspi, P.S. Smith, H. Netzer, D. Maoz, B.T. Jannuzi, & U. Giveon, Astrophys. J., **533**, 631 (2000).
W. Kollatschny, Astron. Astrophys., **407**, 461 (2003a).
W. Kollatschny, Astron. Astrophys., **412**, L61 (2003b).
J.A. Kollmeier et al., Astrophys. J., **648**, 128 (2006).
A.P. Koratkar & C.M. Gaskell, Astrophys. J., **370**, L61 (1991).
J. Kormendy & D. Richstone, ARAA, **33**, 581 (1995).
C.A. Kuehn, J.A. Baldwin, B.M. Peterson, & K.T. Korista, Astrophys. J., **673**, 69 (2008).
H. Landt, M.C. Bentz, B.M. Peterson, M. Elvis, M.J. Ward, K.T. Korista, & M. Karovska, MNRAS, **413**, L106 (2011).
A. Laor, Astrophys. J., **505**, L83 (1998).
D. Lynden-Bell, Nature, **223**, 690 (1969).
F. Macchetto, A. Marconi, D.J. Axon, A,. Capetti, W. Sparks, & P. Crane, Astrophys. J., **489**, 579 (1997).
J. Magorrian et al., Astron. J., **115**, 2285 (1998).
D. Maoz et al., Astrophys. J., **404**, 576 (1993).
A. Markowitz et al., Astrophys. J., **593**, 96 (2003).
A. Marconi, D.J. Axon, R. Maiolino, T. Nagao, G. Pastorini, P. Pietrini, A. Robinson, & G. Torricelli, Astrophys. J., **678**, 693 (2008).
N.J. McConnell & C.-P. Ma, submitted to Astrophys. J., [arXiv:1211.2816] (2013).
K.L. McGill, J.-H. Woo, T. Treu, & M.A. Malkan, Astrophys. J., **673**, 703 (2008).
I.M. McHardy, MNRAS, in press [arXiv:1212.2854] (2013)
I.M. McHardy, E. Koerding, C. Knigge, P. Uttley, & R.P. Fender, Nature, **444**, 730 (2006).
R.J. McLure & M.J. Jarvis, MNRAS, **337**, 109 (2002).
L. Meyer, A.M. Ghez, B. Schödel, S. Yelda, A. Boehle, J.R. Lu, T. Do, M.R. Morris, E.E. Becklin, & K. Matthews, Science, **338**, 84 (2012).
M. Miyoshi, J. Moran, J. Herrnstein, L. Greenhill, N. Nakai, P. Diamond, & M. Inoue, Nature, **373**, 127 (1995).
R. Morales & A.C. Fabian, MNRAS, **329**, 209 (2002).
C.J. Nelson, R.F. Green, G. Bower, K. Gebhardt, & D. Weistrop, Astrophys. J., **615**, 652 (2004).
H. Netzer & P. Marziani, Astrophys. J., **724**, 318 (2010).
C.A. Onken, L.Ferrarese, D.Merritt, B.M. Peterson, R.W. Pogge, M. Vestergaard, & A.Wandel, Astrophys. J., **615**, 645 (2004).
C.A. Onken et al., Astrophys. J., **670**, 105 (2007).
A. Pancoast, B.J. Brewer, & T. Treu, Astrophys. J., **730**:139 (2011).
A. Pancoast et al., Astrophys. J., **754**:49 (2012).
I.E. Papadakis, MNRAS, **348**, 207 (2012).
D. Park, B.C. Kelly, J.-H. Woo, & T. Treu., Astrophys. J. Suppl., **203**:6 (2012).
G. Pastorini et al., Astron. Astrophys., **469**, 405 (2007).
M. Pastoriza & H. Gerola, Astrophys. Letters, **6**, 155 (1970).
B.M. Peterson, PASP, **105**, 247 (1993).
B.M. Peterson, in *Advanced Lectures on the Starburst–AGN Connection*, ed. I. Aretxaga, D. Kunth, & R. Mújica (World Scientific, Singapore, 2001).
B.M. Peterson, L. Ferrarese. K.M. GIlbert, S. Kaspi, M.A. Malkan, D. Maoz, D. Merritt, C.A. Onken, R.W. Pogge, M. Vestergaard, & A. Wandel, Astrophys. J., **613**, 682 (2004).
B.M. Peterson, K.A. Meyers, E.R. Capriotti, C.B. Foltz, B.J. Wilkes, & H.R. Miller, Astrophys. J., **292**, 164 (1985).
B.M. Peterson, R.M. Wagner, D.M. Crenshaw, K.A. Meyers, P.L. Byard, C.B. Foltz, & H.R. Miller, Astron. J., **88**, 926 (1983). d
B.M. Peterson & A. Wandel, Astrophys. J., **521**, L95 (1999).

B.M. Peterson & A. Wandel, Astrophys. J., **540**, L13 (2000).
B.M. Peterson et al., Astrophys. J., **368**, 119 (1991).
B.M. Peterson et al., Astrophys. J., **632**, 799 (2005).
L.Č. Popović et al., Astron. Astrophys., **529**:A130 (2011).
A. Rafiee & P. Hall, Astrophys. J. Suppl., **194**, 42 (2011).
M.J. Rees, ARAA, **22**, 471 (1984).
G.T. Richards et al., Astron. J., **141**:167 (2011).
E.E. Salpeter, Astrophys. J., **140**, 796 (1964).
F. Shankar, New Astron. Rev., **53**, 57 (2009).
A.I. Shapovalova et al., Astron. Astrophys., **509**, 106 (2010).
A.I. Shapovalova et al., Astrophys. J. Suppl., **202**:19 (2012).
Y. Shen, J.E. Greene, M.A. Strauss, G.T. Richards, & D.P. Schneider, Astrophys. J., **680**, 169 (2008).
Y. Shen & B.C. Kelly, Astrophys. J., **746**, 169 (2012).
C.L. Steinhardt & M. Elvis, MNRAS, **402**, 2637 (2010).
C. Siopsis et al., Astrophys. J., **693**, 946 (2009).
J. Thomas, R.P. Saglia, R. Bender, D. Thomas, K. Gebhardt, J. Magorrian, & D. Richstone, MNRAS, **353**, 391 (2004).
J. Tohline & D.E. Osterbrock, Astrophys. J., **210**, L117 (1976).
H.D. Tran, Z. Tsvetanov, H.D. Ford, J. Davies, W. Jaffe, F.C. van den Bosch, & A. Rest Astron. J., **121**, 2928 (2001).
S. Tremaine et al., Astrophys. J., **574**, 740 (2002).
M.-H. Ulrich, A. Boksenberg, M.V Penston, G.E. Bromage, J. Clavel, A. Elvius, G.C. Perola, & M.A.J. Snijders, Astrophys. J., **382**, 483 (1991).
M.-H. Ulrich & K. Horne 1996, MNRAS, **283**, 748 (1996).
M. Valluri, D. Merritt, & E. Emsellem, Astrophys. J., **602**, 66 (2004).
D.E. Vanden Berk, C. Yip, A. Connolly, S. Jester, & C. Stoughton in *AGN Physics with the Sloan Digital Sky Survey*, ed. G.T. Richards & P.B. Hall (Astronomical Society of the Pacific, San Francisco, 2004).
R.P. van der Marel, N. Cretton, P.T. de Zeeuw, & H.-W. Rix, Astrophys. J., **493**, 613 (1998).
M. Vestergaard, Astrophys. J., **571**, 733 (2002).
M. Vestergaard, Astrophys. J., **601**, 676 (2004).
M. Vestergaard & P.S. Osmer, Astrophys. J., **699**, 800 (2009).
M. Vestergaard & B.M. Peterson, Astrophys. J., **625**, 688 (2005).
M. Vestergaard & B.M. Peterson, Astrophys. J., **641**, 676 (2006).
A. Wandel, B.M. Peterson, & M.A. Malkan, Astrophys. J., **526**, 579 (1999).
I. Wanders et al., Astrophys. J., **453**, L87 (1997).
D. Watson, K.D. Denney, M. Vestergaard, & T.M. Davis, Astrophys. J., **740**, L49 (2011).
L.C. Watson, P. Martini, K.M. Dasyra, M.C. Bentz, L. Ferrarese, B.M. Peterson, R.W. Pogge, & L. Tacconi, Astrophys. J., **682**, L21 (2008).
J. Woo et al., Astrophys. J., **716**, 269 (2010).
X.-B. Wu, R. Wang, M.Z. Kong, F.K. Liu, & J.L. Han, Astron. Astrophys., **424**, 793 (2004).
Ya.B. Zel'dovich & I.D. Novikov, Sov. Phys. Dokl., **158**, 811 (1964).
Y. Zu, C.S. Kochanek, & B.M. Peterson, Astrophys. J., **735**:80 (2011).